18th Australasian Fluid Mechanics Conference
Launceston, Australia
3-7 December 2012

The Impacts of Scale Resolutions on the Turbulent Flow Over a Rough Backward-facing Step

Yanhua Wu[1], Huiying Ren[2], Hui Tang[1]

[1]School of Mechanical and Aerospace Engineering
Nanyang Technological University, Singapore, 639798

[2]Hydrology Technical Group
Pacific Northwest National Laboratory, Richland, WA, 99352, USA

Abstract

PIV measurements are performed in the streamwise–wall-normal planes in turbulent flows over a rough backward-facing step (BFS) and two of the step's coarse-scale approximations. The roughness topography is replicated from real turbine blades and its coarse-scale representations are obtained from a multi-resolution analysis using discrete wavelet transform. The experiments are conducted at Re_h=3450 and δ/h=8, where h is the mean step height and δ is the incoming boundary layer thickness. The impacts of the roughness scale resolutions on the BFS turbulent flows are investigated by examining the mean flow structures and the turbulence kinetic energy ($\langle u'^2 + v'^2 \rangle$) distributions.

Introduction

Quite a few recent studies [10, 11, 12, 6, 7] have focused on the impacts of realistic roughness on turbulent flows since many wall-bounded internal and external engineering flows will encounter the irregular and three-dimensional roughness of the surfaces roughened by various damage mechanisms after some time of operation. For a realistic rough surface, it usually possesses a wide range of the topographical length scales. Therefore it is of particular interest to understand the relative impacts of different scales of the roughness topography on the turbulent flows and some research efforts [9, 2, 3, 6] have been undertaken to address such an issue. Further, a turbulent flow over a rough backward-facing step may be used to model the flows at the surface transition from elevated rough-wall to smooth-wall as in cascades of roughened turbine blades as well as flows in various engineering configurations such as diffusers, combustors, airfoils and buildings. The present effort explores the relative impacts of scale resolutions of a realistic roughness on the turbulent backward-facing step (BFS) flows. The roughness was replicated from a land-based turbine blade roughened by deposition of foreign materials. Models with different scale resolutions of this roughness were produced by applying a novel method using discrete wavelet transform, as described in the following section.

Multi-resolution analysis of the roughness topography

Multi-resolution analysis (MRA) is an algorithm proposed by Mallat [5] to efficiently perform discrete wavelet transform of a signal. The discrete wavelet transform of a one-dimensional function $f(t)$ is given as

$$W(j,k) = \int_{-\infty}^{\infty} f(t)\overline{\Psi}_{j,k}(t)dt \tag{1}$$

where $W(j,k)$ are discrete wavelet coefficients and $\Psi_{j,k}(t)$ is a family of discrete wavelet functions given by

$$\Psi_{j,k}(t) = 2^{-j/2}\Psi\left(\frac{t-2^j k}{2^j}\right), \tag{2}$$

and the overbar denotes the complex conjugate.

In MRA, a signal can be decomposed at different resolution levels. At each level, the signal is represented by a low-resolution approximation plus the details on that level and on all other higher resolution levels. That is,

$$f(t) = A_i(t) + \sum_{k=1}^{i} D_k(t), \tag{3}$$

where $A_i(t)$ is the approximation at level i and $D_k(t)$ is the detail at level k. The approximation $A_i(t)$ can be computed by

$$A_i(t) = \sum_{k=-\infty}^{\infty} C_{i,k}^A \cdot \phi_{i,k}(t), \tag{4}$$

where

$$\phi_{i,k}(t) = 2^{-i/2}\phi(\frac{t-2^i k}{2^i}) \tag{5}$$

is a set of orthonormal basis generated from the scaling function, $\phi(t)$, which is a companion function of the wavelet function. $C_{i,k}^A$ are the coefficients obtained by projecting $f(t)$ on the basis $\phi_{i,k}(t)$, i.e., $C_{i,k}^A = \int f(t) \cdot \phi_{i,k}(t)dt$. For a two-dimensional function such as the fluctuating roughness height in this study, approximations at different scale resolution levels can be obtained from a two-dimensional scaling function $\phi(x,y) = \phi(x)\phi(y)$.

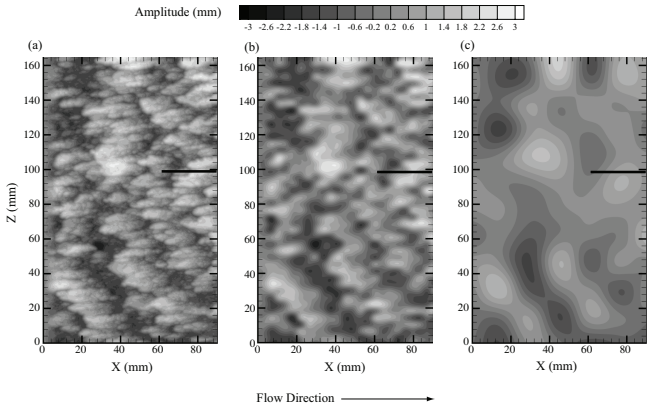

Figure 1: Contour plots of fluctuation heights of (a) the fully rough surface; (b) surface at resolution level 4, A_4; and (c) surface at resolution level 6, A_6. The black lines mark the position of PIV measurement on each surface.

In this study, coarse-scale models at resolution levels of six and four, i.e. surfaces A_6 and A_4, are used together with the original fully rough surface to investigate the impacts of roughness scales on the turbulent boundary layers over backward-facing steps. The contours of the fluctuation heights of these three rough surfaces are presented in figure 1. For roughness approximation A_6, the average peak-to-valley roughness height

is $k = 2.34$ mm and the RMS height is $k_{rms} = 0.64$ mm. For roughness approximation A_4, $k = 4.01$ mm and $k_{rms} = 0.94$ mm. $k = 4.2$ mm and $k_{rms} = 1.0$ mm for the full roughness.

The rough blocks, including A_6, A_4 and the fully rough surface, are fabricated using an Eden 350 3D printer with a resolution of 16 microns at the MechSE Ford Lab at the University of Illinois at Urbana-Champaign. The top surfaces of these blocks are rough while the bottom surfaces are smooth. They are spray painted black in order to reduce the reflection of the laser light sheet during PIV measurements. These blocks are 90 mm (14 h) long, 169 mm (27 h) wide and with the same mean height of $h = 6.35$ mm.

Experiments

The particle image velocimetry (PIV) experiments were performed in an Eiffel-type, open circuit, boundary layer wind tunnel with a freestream turbulence intensity of ∼0.45%. The test section is 67×67 cm in cross-section and 3 m in length within which a 2.90 m long hydraulically smooth flat plate with an elliptically shaped leading edge is suspended 90 mm above the floor of the tunnel. The boundary layer is tripped by a cylindrical rod placed just downstream of the leading edge of the plate. A 100mm-long tail flap is attached to the trailing edge of the plate and is set at $\sim 5^\circ$ in the present experiments to prevent separation at the leading edge of the plate. The physical growth of the boundary layer and the inclined tail flap created a slight favorable pressure gradient with the acceleration parameter $K \equiv \frac{\nu}{U_\infty^2}\frac{dU_\infty}{dx} < 7.0 \times 10^{-8}$ at the measurement location, where U_∞ is the freestream velocity and ν is the kinematic viscosity of the air. The rough block was placed at the spanwise center of the boundary layer plate at about 2.50 m downstream of the leading edge. The resulted aspect ratio (channel width/step height) and expansion ratio are 96 and 1.01, respectively. Two other smooth blocks with the same heights of 6.35 mm are placed along the sides of this rough block to cover the whole width of the wind tunnel.

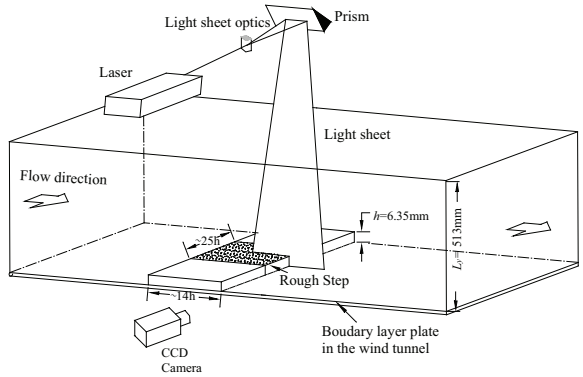

Figure 2: Schematic of experimental setup.

Two-dimensional PIV measurements were performed in the streamwise–wall-normal $(x-y)$ planes as marked in figure 1 for each rough step at $Re_h = \frac{U_\infty h}{\nu} = 3450$, where U_∞ is the freestream velocity, h is the mean step height, and ν is the kinematic viscosity of the air. The flow was seeded with 1 μm olive oil droplets generated by a Laskin nozzle. The flow field was illuminated through the transparent glass ceiling with a 200μm-thick laser sheet generated by a pair of Nd:YAG lasers. An 8-bit frame-straddle CCD camera of 1600 × 1200 pixels was used in conjunction with a 105 mm lens, yielding a filed of view of $\sim 6h \times 3.8h$ (streamwise × wall-normal) and an imaging resolution of about 50 pixels/mm. Measurements were first made in the upstream region of the steps and then the camera was moved to measure the flow fields downstream of the steps. More than one thousand pairs of particle images are acquired for each measurement. The pairs of PIV images were interrogated using a recursive two-frame cross-correlation method with interrogation window size of 20 × 20 pixels with 50% overlap. The resulting velocity vector fields have a grid spacing of 0.2 mm or $h/32$. The vector fields are also validated using objective statistical methods such as magnitude difference and median comparison to remove erroneous velocity vectors. On average, 97-99% of the velocity vectors in any given velocity realization are found to be valid minimizing the need for interpolation of holes. Finally, each vector field is low pass filtered to remove noise associated with frequencies higher than the sampling frequency of the interrogation. The upstream approaching smooth-wall turbulent boundary layer was also measured using PIV at 50 h ahead of the smooth and rough steps. The turbulence statistics of the measured upstream boundary layer was not found to be altered due to the presence of the steps. The Reynolds number based on the momentum thickness of the approaching boundary layer is $Re_\theta = 3130$. The ratio of the upstream boundary layer thickness δ to the mean step height h, δ/h, is 8.

Note that there are two important particularities of the current configuration different from the canonical backward-facing step flows. First, the present study has a small expansion ratio and a large δ/h ratio because the major motivation of this study is to investigate the turbulent boundary layer over the surface transition from an elevated rough wall to a smooth wall. Second, the self-similar upstream boundary layer flows over a short strip of block of about 14h long before it is separated at backward-facing step. Such non-equilibrium boundary layers occur in many engineering flow systems such as the one over a rough turbine blade.

Results and discussion

The measured mean velocity fields over the fully rough backward-facing step and its two coarse-scale resolution models A_6 and A_4 are presented in figure 3. In order to highlight the mean flows within the recirculation region, only those velocity vectors whose streamwise velocities, U, are less than $0.2U_\infty$ are shown. The more uniform flows above the shear layer and upstream of the steps are only represented by the streamlines. The dashed lines are the contour lines where $U = 0$, which can infer the mean reattachment length. The recirculation region below the separated shear layer as well as the secondary bubble in the step's corner are clearly observed in the turbulent BFS flows with different roughness scales. The mean flow structures shown are qualitatively similar to that over a smooth BFS as reviewed in [1]. However, due to the different roughness scales embodied in each rough step, the mean flows illustrate some noticeable differences.

One of the most important parameters in characterizing the mean BFS flow is the reattachment length, X_r, which is determined here to be from the step's edge to the position where the mean streamwise velocity is equal to zero at the first grid point from the wall. Since the first grid point is slightly away from the wall due to the laser reflection during PIV measurements, the values of X_r will be slightly lower than the true values. For the very coarse step model A_6 which includes only large-scale but low amplitude roughness, figure 3 (a) show that X_r is about 4.5h which is similar to the value of 4.8h measured by Kostas ([4]) in a smooth BFS flow with $\delta/h = 5.25$, expansion ratio of 1.02 and aspect ratio of 62. When more small-scale but relatively high-amplitude roughness features are added in step model A_4, the BFS flow over A_4 (figure 3 (b)) illustrated a reattachment

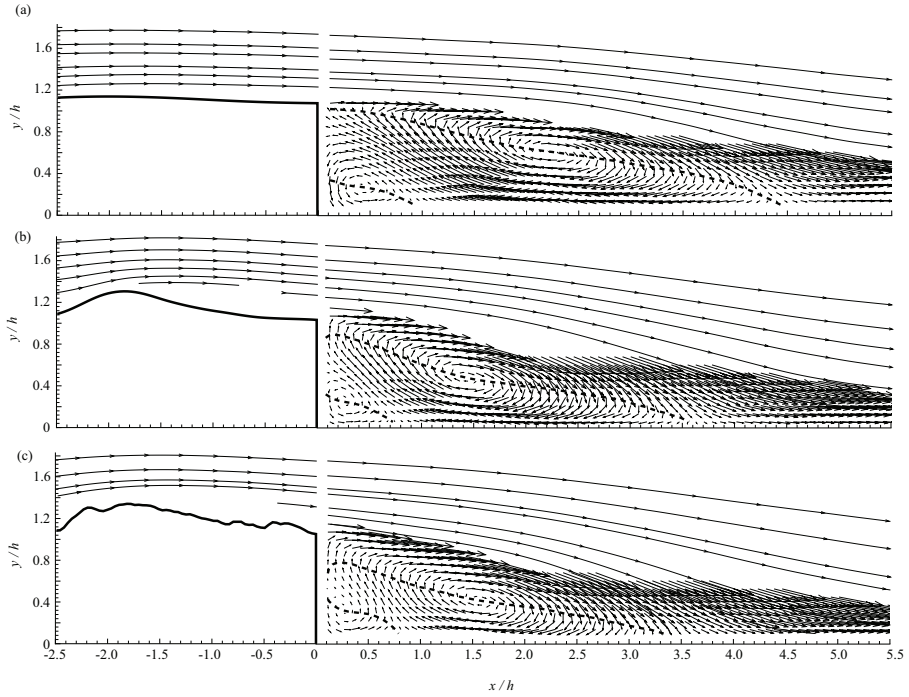

Figure 3: Mean velocity fields over (a) coarse-scale backward-facing step model A_6; (b) coarse-scale backward-facing step model A_4; and (c) fully rough backward-facing step. The flow direction is from left to right. Every other velocity vectors are shown for clarity. Only those velocity vectors whose streamwise velocities, U, are less than $0.2U_\infty$ are shown in order to illustrate the mean flow in the recirculation region. The more uniform flows above the shear layer and upstream of the steps are represented by streamlines. The dashed lines mark the locations where $U = 0$.

length of $3.5h$, more than 20% shorter than X_r for A_6. The reason for the decrease in X_r may lie in the fact that the streamlines ahead of the step A_4 is curved down much more dramatically than those for A_6 due to the specific roughness feature in A_4 at the measurement location. Figure 3 (c) shows that X_r for the fully rough step is about $3.4h$, which is essentially the same as that for step A_4 when the measurement uncertainty of about $0.2h$ is taken into consideration. Therefore, the fine scale roughness between A_4 and the full roughness at the measurement location does not appear to affect the mean reattachment length although roughness profiles between these two cases are still quite distinct in that A_4 reaches a plateau just ahead of the BFS while an obvious downward slope exists in the fully rough step before the flow separates.

Also shown in figure 3 is that the central locations of the primary recirculation bubbles are affected by the roughness scales albeit by different amounts. From A_6 to A_4, the center of the primary bubble moves upstream closer to the step and downward closer to the bottom wall, probably due to the curved streamlines ahead of the step for A_4. On the other hand, the difference in locations of the bubbles between A_4 and the fully rough step is only slight. Since the primary recirculation bubbles for A_4 and the fully rough step are closer to the step than that for A_6, the secondary recirculation bubble is found to be slightly longer in the streamwise direction for the A_6 case than the other two cases. However, the effects of the roughness scales on the secondary recirculation bubbles are much smaller than on the primary bubbles.

The turbulence kinetic energy (TKE) $\langle u'^2 + v'^2 \rangle / U_\infty^2$ is presented in figure 4 for all three scale-resolutions of the rough backward-facing step. Since the two-dimensional PIV performed in this study did not yield the spanwise velocity component, the contribution to the kinetic energy from $\langle w'^2 \rangle$ is neglected here. TKE for the A_6 step as presented in figure 4 (a) is qualitatively similar to other results on smooth BFSs [8, 4, 1]. Significant levels of turbulence is produced after the flow is separated from the BFS of A_6 in the vicinity of the shear layer. Maximum TKE occurs at about $1h$ upstream from the mean reattachment point and relevant constant TKE is observed between $3 \sim 4h$. However, the turbulence level close to the step's corner is very low and is consistent with what was described as a "laminar like" flow in other studies. Upstream of the A_6 step before the flow separation, there exists a region with slightly higher TKE (> 0.016 in figure 4 (a)) which is actually a reminiscent of the high TKE produced by the forward-facing step of the block. The result shown in figure 4 (a) therefore shows that the large-scale but low-amplitude roughness does not appear to affect the turbulence in the BFS flow very much.

However, figure 4 (b) shows that the turbulence is significantly reduced by the smaller-scale roughness included in step A_4. The maximum TKE for step A_4 is about 15% smaller than that for A_6 and its location is shifted to about $1h$ downstream of the reattachment point. High levels of TKE do not appear to originate from the backward-facing step as in the A_6 case or in other smooth step flows. Instead, the region with high levels of TKE after the step seems connected to the small separation region from the roughness bump ahead of the step at about $-2h$. The adverse pressure gradient produced in the small separation between $-2h$ and the step may slightly reduce the strong adverse pressure encountered by the flow after the step and therefore reduce the turbulence levels. It can also be observed that TKE above and upstream the step is stronger for A_4 than that for A_6. It is interesting to notice that above the top surface of A_4, lower turbulence is produced near the ridge of the roughness while higher turbulence exists in the roughness valley, which

may be explained by the local pressure gradients caused by the roughness profiles. The comparison between figure 4 (b) and (c) reveals that the differences in TKE between A_4 and fully rough step cases are quite small. It can only be observed that the slightly elevated turbulence above the fully rough step's top surface extends a little further downstream and the region with normalized TKE larger than 0.03 is a little larger in the recirculation flow. These results show that the fine roughness scales excluded in A_4 at the measurement location have little effects on the turbulence kinetic energy.

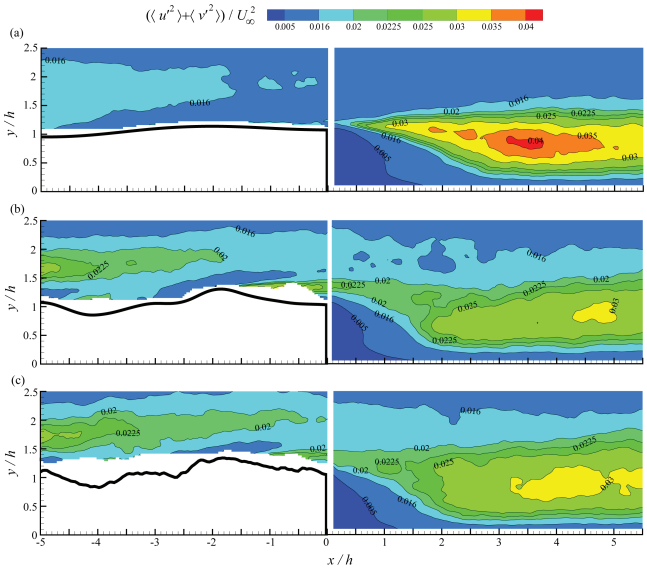

Figure 4: Contour of the kinetic energy $\langle u'^2 + v'^2 \rangle / U_\infty^2$ for (a) coarse-scale backward-facing step model A_6; (b) coarse-scale backward-facing step model A_4; and (c) fully rough backward-facing step.

Summary and conclusions

The impacts of scale resolutions of a realistic roughness on a turbulent backward-facing step flow are explored in this paper through PIV measurements in the streamwise–wall-normal planes. The roughness topography is replicated from real turbine blades and its two coarse-scale models are obtained from a novel method, multi-resolution analysis using discrete wavelet transform. The experiments are performed at $Re_h = 3450$ and $\delta/h = 8$. It was found that the large-scale but low-amplitude roughness scales do not have significant effects on either the mean flow structures or the turbulence kinetic energy of the backward-facing step flows. Further inclusion of smaller-scale but higher-amplitude roughness features to the resolution level four in the current multi-resolution analysis reveals dramatic impacts on the backward-facing step flows. It is found that the mean reattachment length is significantly reduced, possibly because the upstream flow is curved down due to the specific roughness topography at the current measurement location. In addition, the turbulence kinetic energy is dramatically reduced by the smaller roughness features. However, very small impacts are observed to be exerted by finer roughness scales possessed only in the fully rough step studied herein.

In this paper, only the results at one spanwise location are presented because of the page limit for this meeting. Results at another spanwise location are indeed available and will possibly be presented during the oral presentation. The general results are that the effects of the roughness scales depend on the specific roughness topographies at different spanwise locations and therefore the results shown in this paper cannot be generalized into other spanwise positions. Note that the results are indeed particular about the specific roughness. The motivation for choosing the current roughness is that this particular roughness has been shown in the past to have significant detrimental effects on the performance of ground-based turbines. However, the current results indicate that the slope of the roughness may play a major role and further investigations for this as well as other possible dominate roughness parameters are needed.

Acknowledgements

The authors would like to thank Prof. Christensen at the University of Illinois at Urbana-Champaign for providing the full roughness topography data.

References

[1] Eaton, J. and Johnston, J., A review of research on subsonic turbulent flow reattachment., *AIAA Journal*, **19**, 1981, 1093–1100.

[2] Itoh, M., Tamano, S., Iguchi, R., Yokota, K., Akino, N., Hino, R. and Kubo, S., Turbulent drag reduction by the seal fur surface, *Phys. Fluids*, **18**, 2006, 1–9.

[3] Johnson, B. and Christensen, K., Turbulent flow over low-order models of highly-irregular surface roughness., *AIAA J.*, **47**, 2009, 1288–1299.

[4] Kostas, J., Soria, J. and Chong, M., Particle image velocimetry measurements of a backward-facing step flow., *Exp Fluids*, **33**, 2002, 838–853.

[5] Mallat, S., A theory for multiresolution signal decomposition: the wavelet representation., *IEEE Trans. Pattern Anal. Mach. Intell.*, **11**, 1989, 674–693.

[6] Mejia-Alvarez, R. and Christensen, K., Low-order representations of irregular surface roughness and their impact on a turbulent boundary layer., *Physics of Fluids*, **22**, 2010, 015106.

[7] Ren, H. and Wu, Y., Turbulent boundary layers over smooth and rough forward-facing steps., *Phys. Fluids*, **23**, 2011, 045102.

[8] Scarano, F. and Riethmuller, M., Iterative multigrid approach in piv image processing with discrete window offset., *Exp Fluids*, **26**, 1999, 513–523.

[9] Schultz, M. P. and Flack, K. A., Outer layer similarity in fully rough turbulent boundary layers., *Exp. Fluids*, **38**, 2005, 328.

[10] Wu, Y. and Christensen, K. T., Reynolds-stress enhancement associated with a short fetch of roughness in wall turbulence., *AIAA J.*, **44**, 2006, 3098.

[11] Wu, Y. and Christensen, K. T., Outer-layer similarity in the presence of a practical rough-wall topography., *Phys. Fluids*, **19**, 2007, 085108.

[12] Wu, Y. and Christensen, K. T., Spatial structure of a turbulent boundary layer with irregular surface roughness, *J. Fluid Mech.*, **655**, 2010, 380–418.